Supplementary Information

Healable Poly(urethane-urea) Elastomer with Ultra-high Mechanical Strength Enabled by Tailoring Multiple Relaxation Dynamics of Hierarchical Hard Domains

Yue Huang, Haitao Wu, Weihang Li, Zhaoyang Yuan, Qi Wu*, Ruihai Li, Jinrong Wu*

State Key Laboratory of Polymer Materials Engineering, College of Polymer Science and Engineering, Sichuan University, Chengdu 610065, China.

***Corresponding author:** E-mail: wujinrong@scu.edu.cn

1. Experimental Section

1.1. Materials

Polytetramethylene ether glycol (PTMEG, M_n = 2000 g/mol) was purchased from Aladdin, and dried under vacuum at 100 ℃ for 1h to remove residual moisture before use. Other reagents and solvents in the synthesis were used without further purification. Isophorone diisocyanate (IPDI), dibutyltin dilaurate (DBTDL) and 4,4-Diamino-1,2-Diphenylethane (DADPE) were purchased from TCL. 4-amino phenyl disulfide (APS) and anhydrous tetrahydrofuran (THF) were provided by Adamas. 2, 6-pyridinedimethanol (PDM) was purchased from Macklin.

1.2. Synthesis

The synthetic procedure is shown in Fig. S1, and the synthetic formula with components and contents in detail is summarized in Table 1. Taking PUU-$T_{0.6}D_{0.4}$-$I_{2.3}$ as example, a three-neck round bottom flask equipped with a magnetic stirrer was loaded with PTMEG (M_n of 2000 g/mol, 8 g, 0.004 mol) and PDM (0.42 g, 0.003 mol), followed by heating at 80 ℃ under vacuum and stirring for 60 min to remove the moisture. After cooling to 60 ℃, a mixture containing IPDI (3.56 g, 0.016 mol), DBTDL (0.2 ml) and anhydrous THF (40 mL) was added to the flask. Then the whole reaction system was stirred at 60 ℃ under nitrogen atmosphere for 24 h to obtain the first stage product. Subsequently, APS (2.24 g, 0.009 mol) dissolved in 5 mL of anhydrous THF was injected dropwise into the sealed flask for further chain extension. Then the whole system was kept at 60 ℃ under stirring for another 24 h to accomplish complete polymerization. The as-obtained product was precipitated in excess n-hexane and washed several times, followed by drying under vacuum at 60 ℃ to constant weight.

1.3. Film preparation of PUU

A 15 wt% PUU solution was poured into a square Teflon mold with dimensions of 70mm×50mm×10mm. After most of THF volatilized under room temperature for 24 h and 60 ℃ for another 24 h, the mold was dried at 60 ℃ under vacuum to remove the residual solvent. A thin PU film (thickness ≈ 0.6 mm) without bubble was obtained this way.

1.4. Characterizations and Methods

1.4.1. Nuclear Magnetic Resonance (NMR). The ^{1}H NMR spectra were measured on a Bruker AV III HD spectrometer operating at 400 MHz in deuterated methanol solution with tetramethylsilane as reference.

1.4.2. Gel permeation chromatography (GPC). The molecular weight and polydispersity index (PDI) were determined by gel permeation chromatography (GPC), using THF as the eluent.

1.4.3. Fourier transform infrared spectroscopy (FTIR). FTIR spectra was recorded using Nicolet iS10 (Nicolet, America) in the range of 4000-400 cm^{-1} at room temperature. The FTIR samples were prepared by evaporating THF of product solution on a piece of KBr plate. Temperature-dependent FTIR spectra was collected in the range of 30 to 150 °C at a heating rate of 1 °C min^{-1}.

1.4.4. Small-Angle X-ray Scattering (SAXS). SAXS experiments were performed on a Xeuss 3.0 equipment with a X-ray of 0.154 nm. The sample-to-detector distance is 900 mm. One SAXS image was recorded within the exposure time of 10 min by a Eiger2R 1M detector.

1.4.5. Atomic force microscopy (AFM). AFM observation was performed on an AIST controller (Association for Iron & Steel Technology Co. Ltd.) in the tapping mode to analyze the surface morphologies of PU samples, the test samples were dissolved in

THF (6 mg PU in 100mL THF) and dropped on the silicon wafer, then tested directly after solvent volatilization.

1.4.6 Dynamic mechanical analysis (DMA). DMA measurements were performed on the Dynamic Mechanical Analyzer Q800 (TA Instrument, Waters Ltd.) under the tensile mode in a temperature range of -110 to 170 °C at a heating rate of 3 °C min^{-1}. The stress relaxation was performed with a stain of 10% at different temperatures.

1.4.7 Tensile tests. Mechanical properties were measured on a universal testing machine (USA, Instron Instruments, model: 5967) at room temperature with a strain rate of 50 mm min^{-1}. Dumbbell-shaped samples were prepared with central dimensions of 18.0 mm × 2.0 mm × 0.6 mm. Each sample was tested at least three times. For the cyclic tensile test, successive loaded-unloaded cycles were conducted at a strain rate of 50 mm min^{-1} with a maximum strain of 700 %.

1.4.8 Measurement of the fracture energy. The fracture energy test was conducted by the tensile test using the single-edge notched sample of 4 mm in width with a notch of 1 mm. The notched and unnotched specimens (central dimensions of 20.0 mm × 4.0 mm × 0.6 mm) were both tested at the stretching speed of 5 mm min^{-1}. The fracture energy (G_c) was calculated by the following equation:

$$G_c = \frac{6wc}{\sqrt{\lambda_c}}$$

where c represents the length of the slit (1 mm), λc represents the elongation-at- break of the notched sample, w represents the strain energy calculated by integration of the stress-strain curve of the unnotched specimen until ε_c ($\varepsilon_c = \lambda_c - 1$).

1.4.9 Healing ability. To assess the healing capacity, the dumbbell-shaped sample (18.0 mm×2.0 mm×0.6 mm) was cut into two parts by fresh blade, then the fresh cut

surfaces were spliced together by hand. The followed healing processes were carried out in a vacuum oven at different temperature for different time. The healing efficiency is defined as the ratio of the fracture strength of the healed sample to that of the pristine one:

$$Healing\ efficiency = \frac{\sigma_{cut}}{\sigma_{uncut}}$$

where the σ_{cut} refers to the fracture stress of the healed samples, and σ_{uncut} refers to the fracture stress of the uncut samples.

1.4.10. Calculation of activation energy.

The temperature dependence of the relaxation time can be fitted by the Arrhenius equation:

$$ln\tau = ln\tau_0 + \frac{E_a}{RT}$$ where E_a is activation energy, R and T is gas constant and absolute temperature, respectively.

Reference

1 E. Ducrot, Y. Chen, M. Bulters, R. P. Sijbesma and C. Creton, *Science*, 2014, **344**, 186–189.

2 N. Kazem, M. D. Bartlett and C. Majidi, *Adv. Mater.*, 2018, **30**, 1–7.

3 J. Kang, D. Son, G. J. N. Wang, Y. Liu, J. Lopez, Y. Kim, J. Y. Oh, T. Katsumata, J. Mun, Y. Lee, L. Jin, J. B. H. Tok and Z. Bao, *Adv. Mater.*, 2018, **30**, 1–8.

4 J. Wu, L. H. Cai and D. A. Weitz, *Adv. Mater.*, 2017, **29**, 1–8.

5 L. Chen, T. L. Sun, K. Cui, D. R. King, T. Kurokawa, Y. Saruwatari and J. P. Gong, *J. Mater. Chem. A*, 2019, **7**, 17334–17344.

6 X. Yan, Z. Liu, Q. Zhang, J. Lopez, H. Wang, H. C. Wu, S. Niu, H. Yan, S. Wang, T. Lei, J. Li, D. Qi, P. Huang, J. Huang, Y. Zhang, Y. Wang, G. Li, J. B. H. Tok, X. Chen and Z. Bao, *J. Am. Chem. Soc.*, 2018, **140**, 5280–5289.

7 D. Wang, J. H. Xu, J. Y. Chen, P. Hu, Y. Wang, W. Jiang and J. J. Fu, *Adv. Funct. Mater.*, 2020, **30**, 1907109.

8 Y. Li, W. Li, A. Sun, M. Jing, X. Liu, L. Wei, K. Wu and Q. Fu, *Mater. Horizons*, 2021, **8**, 267–275.

9 J. Zhou, D. Shi, Y. Wang, M. Chen and W. Dong, *Mater. Res. Bull.*, 2022, **154**, 111939.

10 D. Wang, Z. Wang, S. Ren, J. Xu, C. Wang, P. Hu and J. Fu, *Mater. Horizons*, 2021, **8**, 2238–2250.

11 Y. Zhu, Q. Shen, L. Wei, X. Fu, C. Huang, Y. Zhu, L. Zhao, G. Huang and J. Wu, *ACS Appl. Mater. Interfaces*, 2019, **11**, 29373−29381.

2. Supplementary Figures and Tables

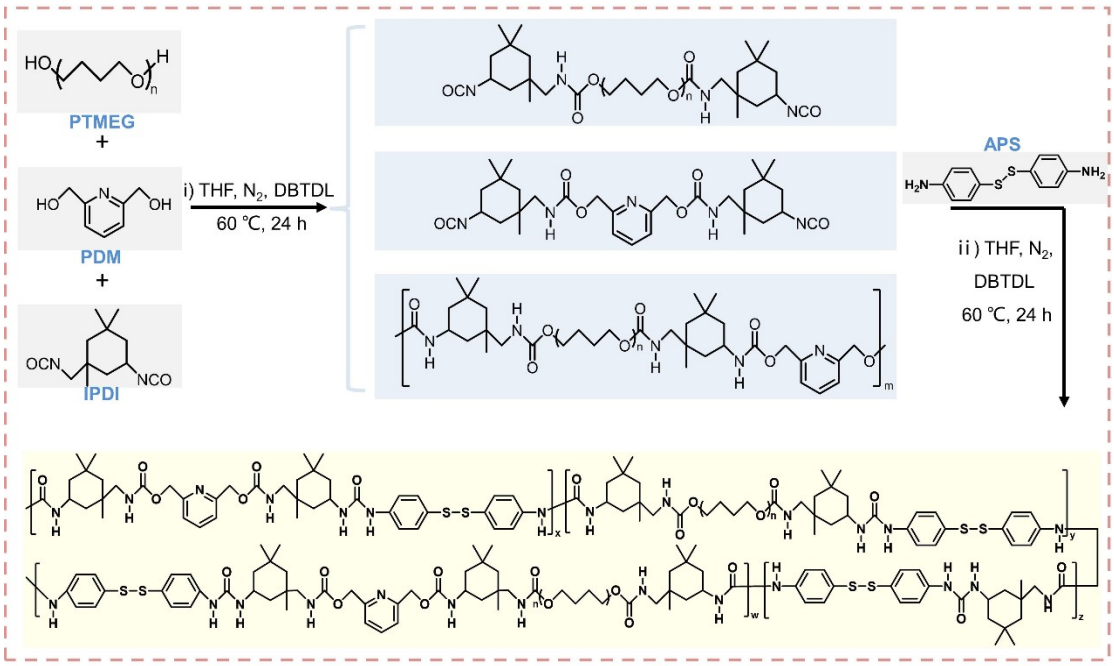

Figure S1 Synthesis route of PUU.

Table S1 Gel permeation chromatography (GPC) results of prepolymers of PUU-$T_{0.5}D_{0.5}$-I_y (y=1.1, 1.7, 2.3, 2.9)

Sample	M_n (g/mol)	M_w (g/mol)	PDI
PUU-$T_{0.5}D_{0.5}$-$I_{1.1}$	102088	187061	1.832
PUU-$T_{0.5}D_{0.5}$-$I_{1.7}$	31095	82732	2.661
PUU-$T_{0.5}D_{0.5}$-$I_{2.3}$	14418	52831	3.664
PUU-$T_{0.5}D_{0.5}$-$I_{2.9}$	7784	18381	2.361

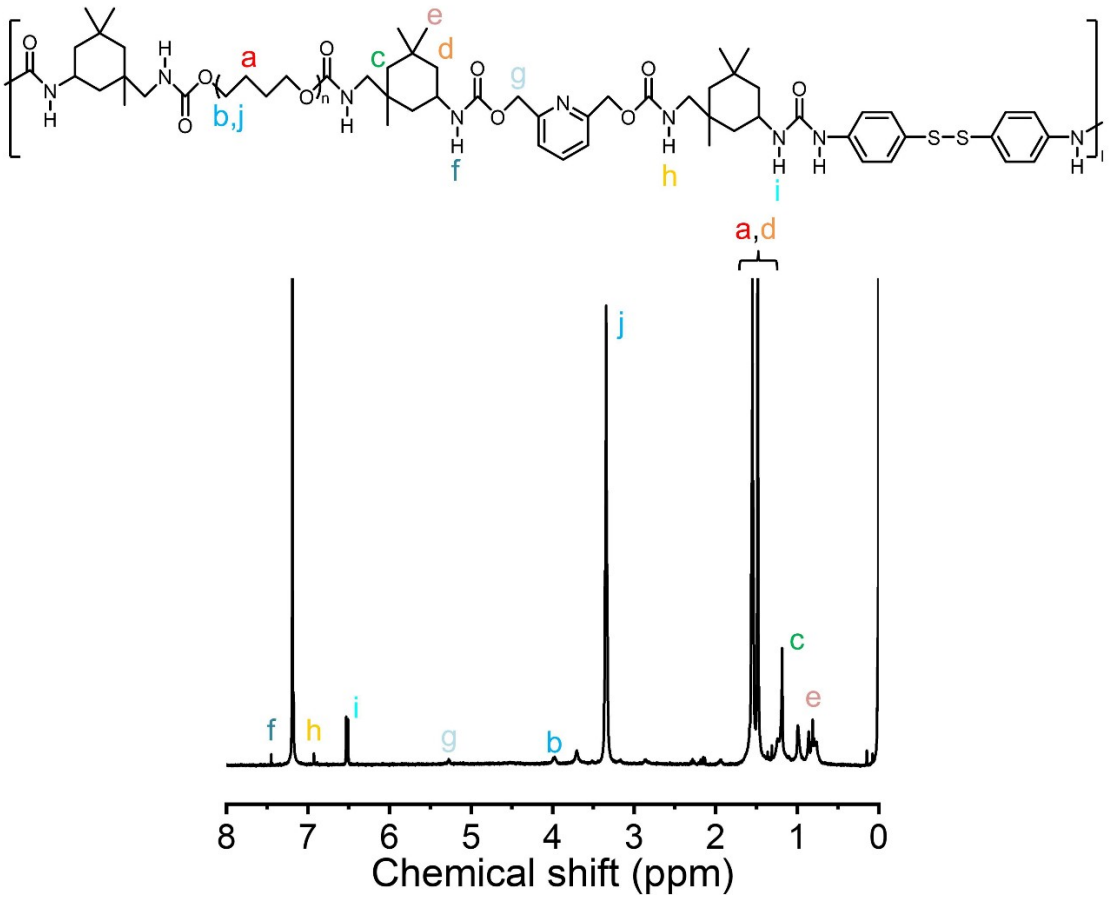

Figure S2 The ^{1}H NMR spectra of PUU-$T_{0.6}D_{0.4}$-$I_{2.3}$

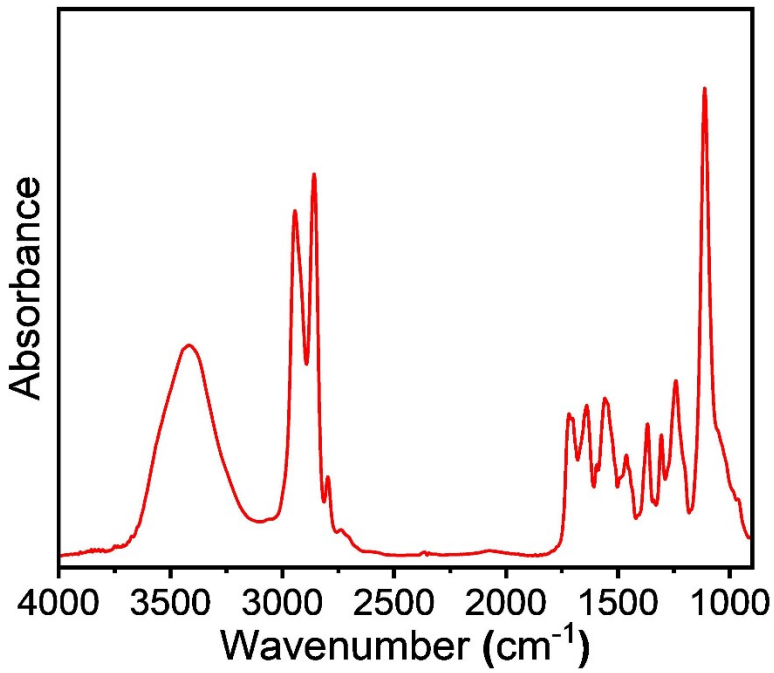

Figure S3 FTIR spectrum of PUU-$T_{0.6}D_{0.4}$-$I_{2.3}$.

Detailed peak assignments are listed in Table S2

Table S2 Characteristic peak assignments of PUU-$T_{0.6}D_{0.4}$-$I_{2.3}$.

Assignments		**Wavenumber (cm^{-1})**
v(N-H)	free	3449
	H-bonded	3360
v_a (CH_2)		2943, 2857
v_s (CH_2)		2796, 2738
v(C=O) urethane	free	1719
	H-bonded	1706
v(C=O) urea	free	1689
	H-bonded	1671, 1652, 1639
Pyridine ring		1462
v(C-N) + δ (N-H) amide	free	1545, 1204
	H-bonded	1559, 1241

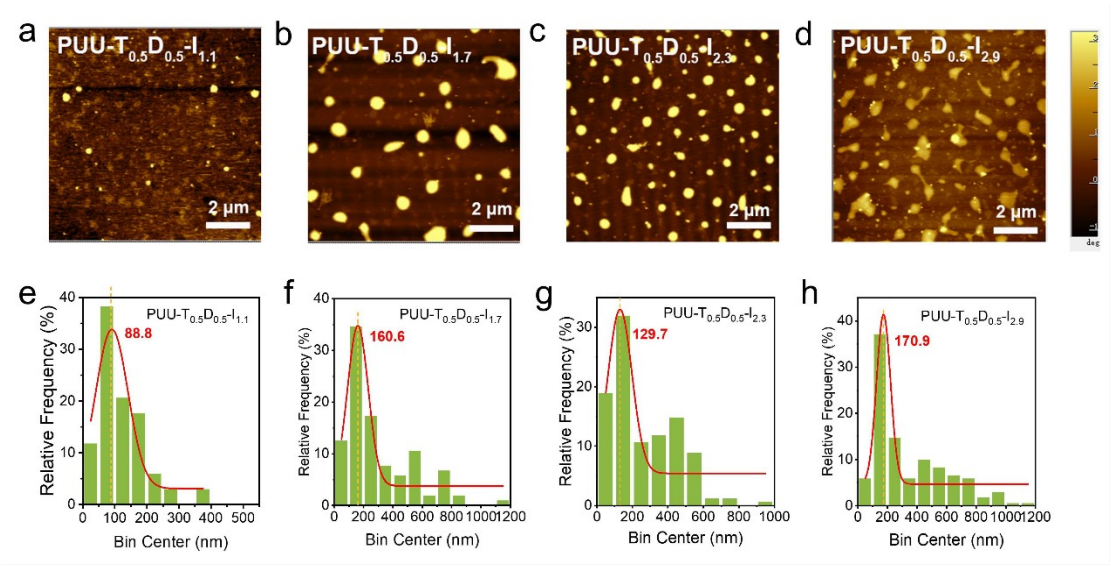

Figure S4 AFM height images of (a) PUU-$T_{0.5}D_{0.5}$-$I_{1.1}$, (b) PUU-$T_{0.5}D_{0.5}$-$I_{1.7}$, (c) PUU-$T_{0.5}D_{0.5}$-$I_{2.3}$ and (d) PUU-$T_{0.5}D_{0.5}$-$I_{2.9}$. Particle size distribution statistics of (e) PUU-$T_{0.5}D_{0.5}$-$I_{1.1}$, (f) PUU-$T_{0.5}D_{0.5}$-$I_{1.7}$, (g) PUU-$T_{0.5}D_{0.5}$-$I_{2.3}$ and (h) PUU-$T_{0.5}D_{0.5}$-$I_{2.9}$ according to AFM images.

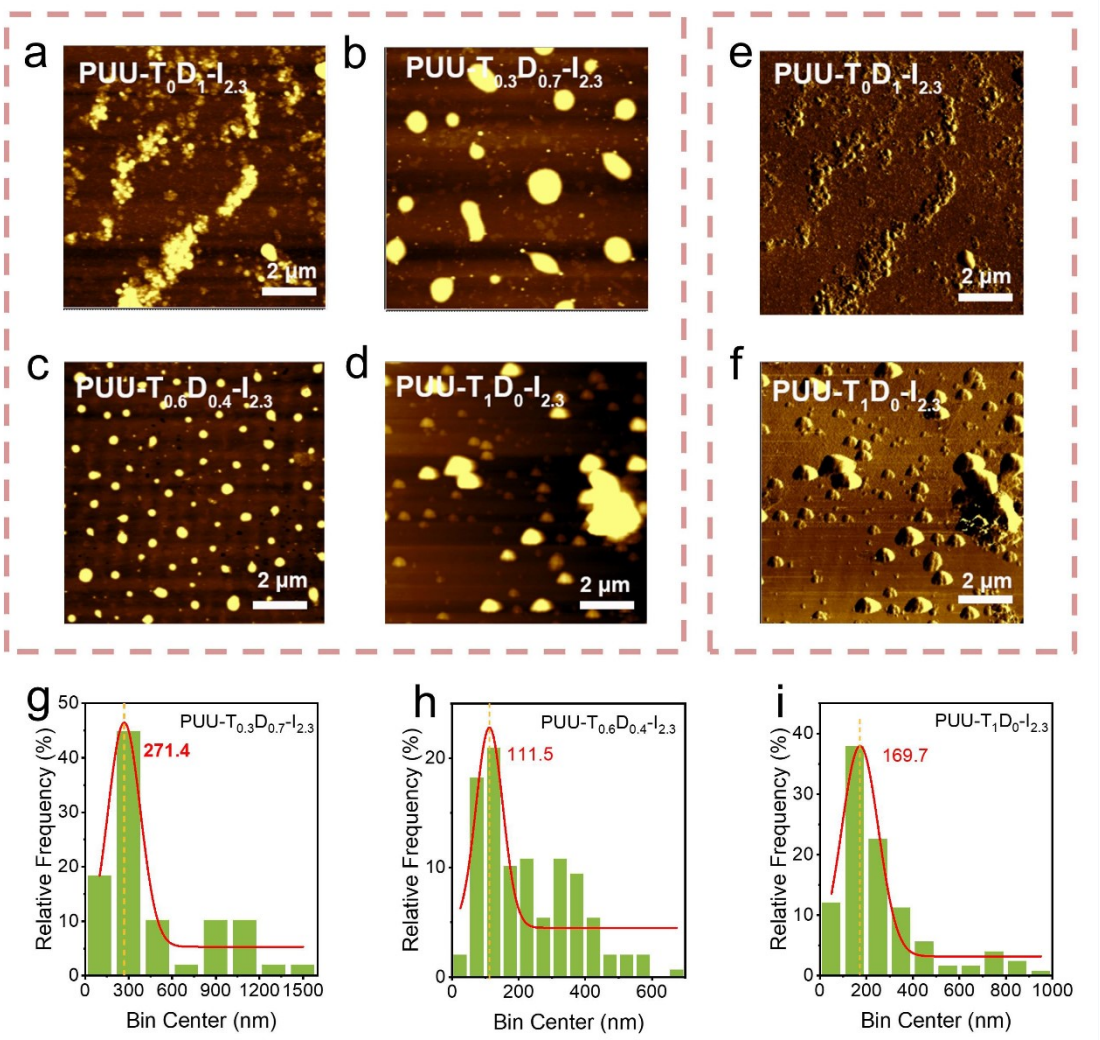

Figure S5 AFM height images of (a) PUU-T_0D_1-$I_{2.3}$, (b) PUU-$T_{0.3}D_{0.7}$-$I_{2.3}$, (c) PUU-$T_{0.6}D_{0.4}$-$I_{2.3}$ and (d) PUU-T_1D_0-$I_{2.3}$. AFM phase images of (e) PUU-T_0D_1-$I_{2.3}$ and (f) PUU-T_1D_0-$I_{2.3}$. Particle size distribution statistics of (g) PUU-$T_{0.3}D_{0.7}$-$I_{2.3}$, (h) PUU-$T_{0.6}D_{0.4}$-$I_{2.3}$ and (i) PUU-T_1D_0-$I_{2.3}$ according to AFM images.

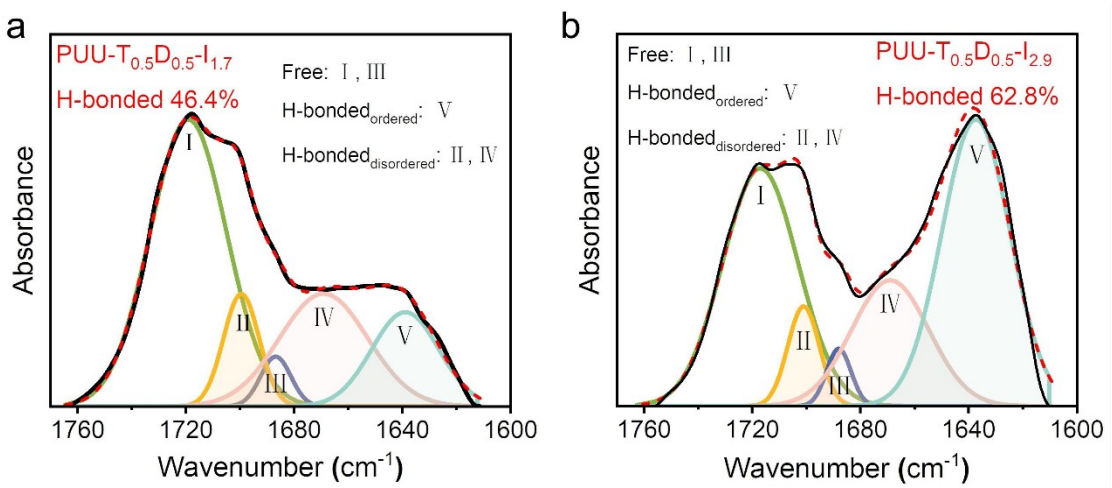

Figure S6 FTIR spectra of (a) PUU-$T_{0.5}D_{0.5}$-$I_{1.7}$ and (b) PUU-$T_{0.5}D_{0.5}$-$I_{2.9}$ in the C=O stretching vibration region.

Table S3 Quantitative analysis of composition of hydrogen bonds in PUU-$T_{0.5}D_{0.5}$-I_y.

		PUU-$T_{0.5}D_{0.5}$-$I_{1.7}$		**PUU-$T_{0.5}D_{0.5}$-$I_{2.3}$**		**PUU-$T_{0.5}D_{0.5}$-$I_{2.9}$**	
free		53.6%		47.8		37.2%	
H-bonded	**ordered**	46.4%	14.5%	52.2%	26.3%	62.8%	37.9%
	disordered		31.9%		38.6%		24.9%

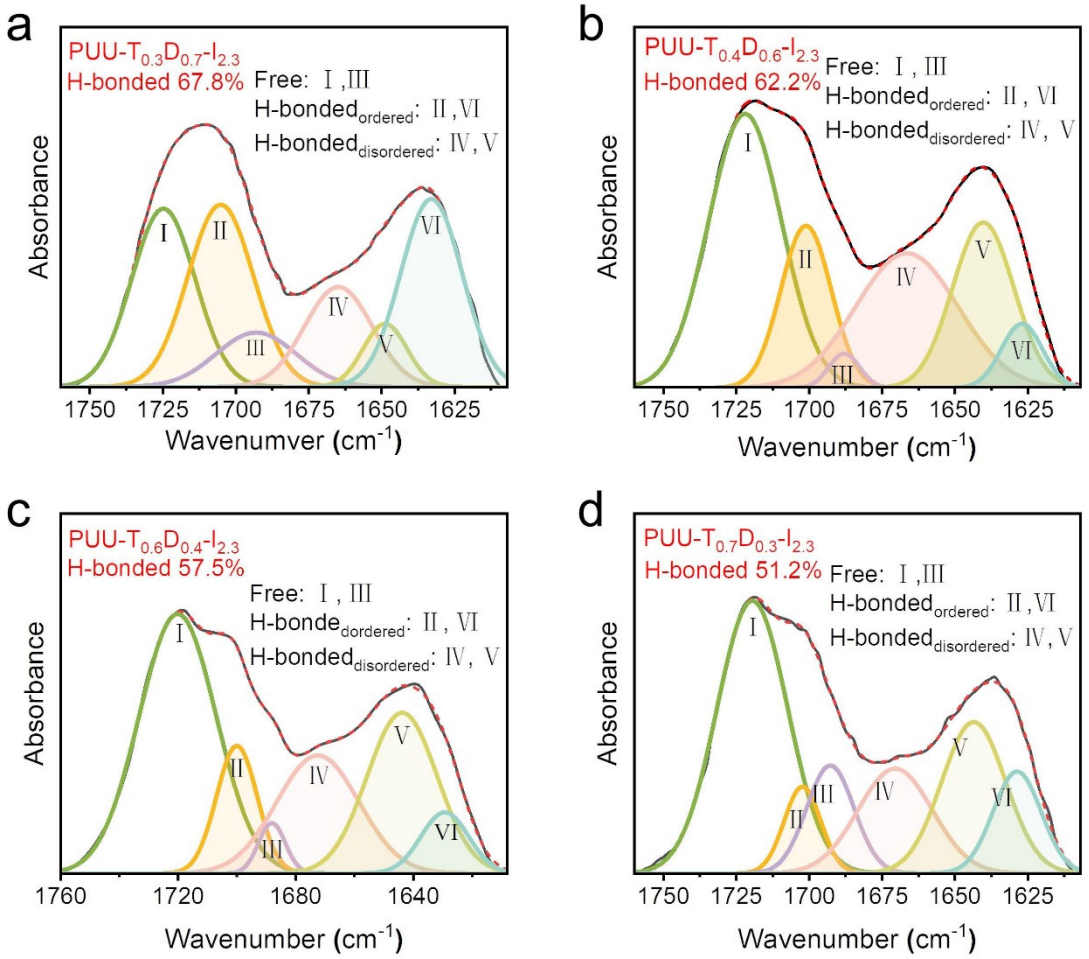

Figure S7. FTIR spectra of (a) PUU-$T_{0.3}D_{0.7}$-$I_{2.3}$, (b) PUU-$T_{0.4}D_{0.6}$-$I_{2.3}$, (c) PUU-$T_{0.6}D_{0.4}$-$I_{2.3}$ and (d) PUU-$T_{0.7}D_{0.3}$-$I_{2.3}$ in the C=O stretching vibration region.

Table S4 Quantitative analysis of composition of hydrogen bonds in PUU-$T_{0.5}D_{0.5}$-$I_{2.3}$.

		PUU-$T_{0.3}D_{0.7}$-$I_{2.3}$		PUU-$T_{0.4}D_{0.6}$-$I_{2.3}$		PUU-$T_{0.6}D_{0.4}$-$I_{2.3}$		PUU-$T_{0.7}D_{0.3}$-$I_{2.3}$	
free		32.2%		37.8%		42.4%		48.8%	
H-bonded	**ordered**	67.8%	48.2%	62.2%	19.4%	57.6%	16.0%	51.2%	16.2%
	disordered		19.6%		42.8%		41.6%		35.0%

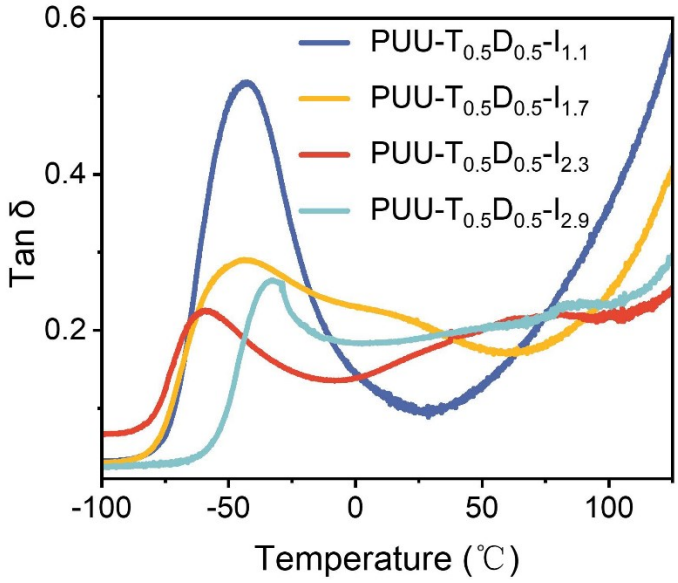

Figure S8 Temperature-dependence of loss factors of PUU-$T_{0.5}D_{0.5}$-I_y.

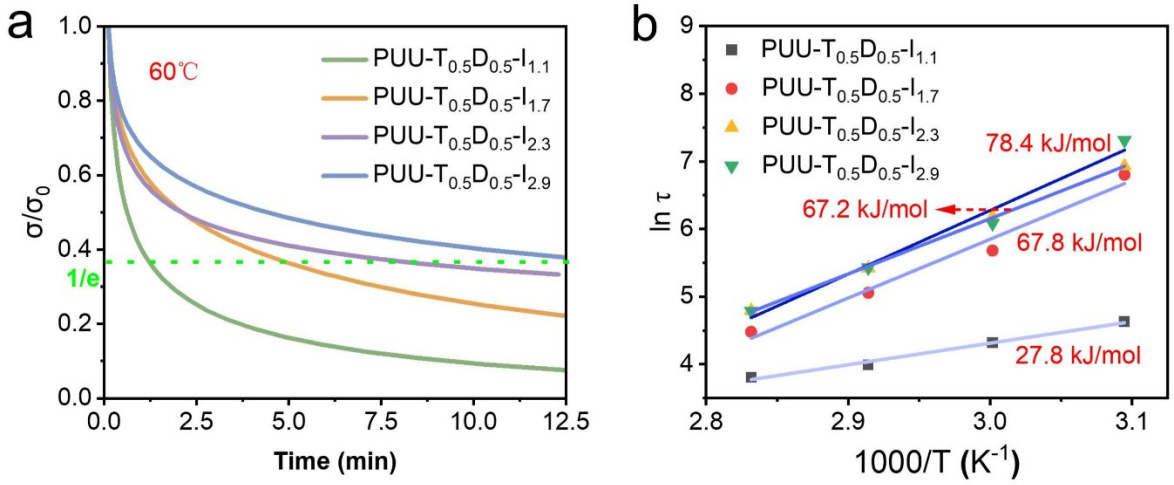

Figure S9 (a) Normalized stress relaxation curves of PUU-$T_{0.5}D_{0.5}$-I_y (y=1.1, 1.7, 2.3 2.9). (b) Fittings of the relaxation time of PUU-$T_{0.5}D_{0.5}$-I_y (y=1.1, 1.7, 2.3 2.9) according to the Arrhenius's law.

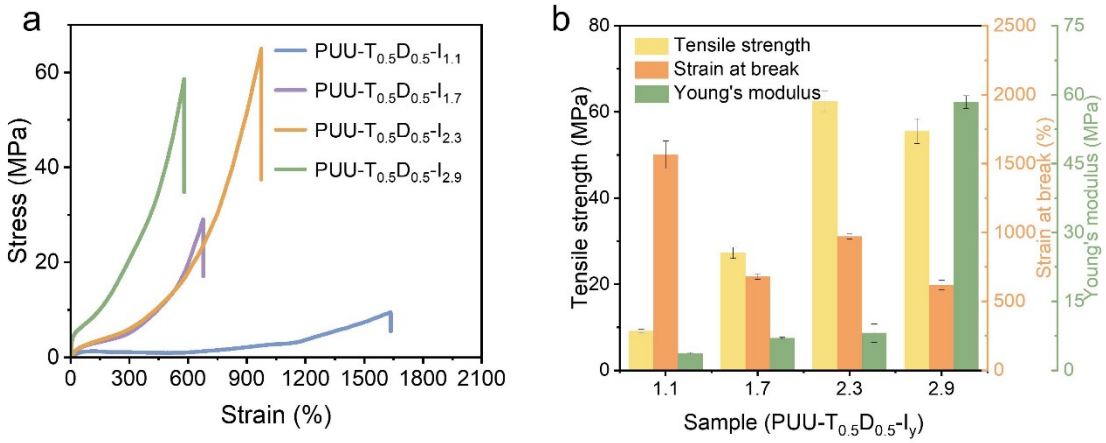

Figure S10. Representative stress-strain curves of PUU-$T_{0.5}D_{0.5}$-I_y. (b) Summary of mechanical properties of PUU-$T_{0.5}D_{0.5}$-I_y.

Table S5 Mechanical properties of PUU-$T_{0.5}D_{0.5}$-I_y.

Sample	Tensile stress (MPa)	Strain at break (%)	Young's modulus (MPa)	Toughness (MJ/m^3)
PUU-$T_{0.5}D_{0.5}$-$I_{1.1}$	9.1 ± 0.5	1563.9 ± 100.1	3.7 ± 0.2	45.2 ± 2.5
PUU-$T_{0.5}D_{0.5}$-$I_{1.7}$	27.3 ± 1.3	679.6 ± 20.1	7.0 ± 0.2	58.7 ± 4.8
PUU-$T_{0.5}D_{0.5}$-$I_{2.3}$	62.4 ± 2.5	971.1 ± 17.9	8.1 ± 1.4	175.1 ± 8.2
PUU-$T_{0.5}D_{0.5}$-$I_{2.9}$	55.5 ± 2.9	619.4 ± 35.3	58.4 ± 2.0	141.4 ± 13.5

Table S6 Mechanical properties of PUU-T_xD_{1-x}-$I_{2.3}$.

Sample	Tensile stress (MPa)	Strain at break (%)	Young's modulus (MPa)	Toughness (MJ/m^3)
PUU-$T_{0.3}D_{0.7}$-$I_{2.3}$	44.4 ± 1.5	663.4 ± 6.4	69.3 ± 0.8	117.6 ± 5.1
PUU-$T_{0.4}D_{0.6}$-$I_{2.3}$	66.8 ± 2.2	683.3 ± 10.2	72.9 ± 0.6	172.0 ± 7.9
PUU-$T_{0.6}D_{0.4}$-$I_{2.3}$	75.8 ± 0.9	711.0 ± 13.0	27.2 ± 0.9	171.4 ± 4.2
PUU-$T_{0.7}D_{0.3}$-$I_{2.3}$	28.0 ± 2.4	871.2 ± 13.8	5.1 ± 0.3	71.1 ± 0.7
PUU-T_1D_0-$I_{2.3}$	28.1 ± 3.4	958.7 ± 10.0	5.2 ± 0.5	70.3 ± 7.5

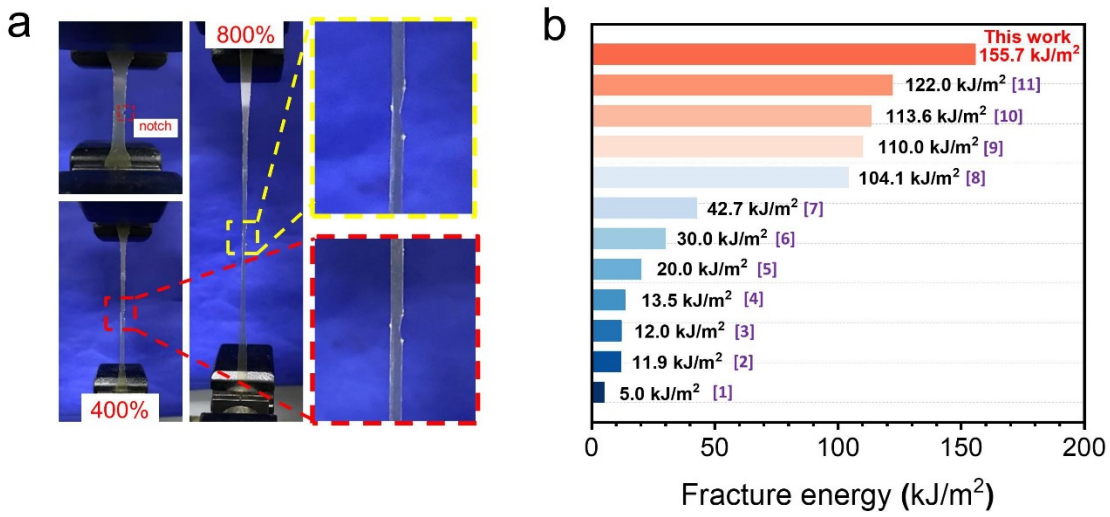

Figure S11 (a) Photographs of the notched PUU-$T_{0.6}D_{0.4}$-$I_{2.3}$ sample stretched to different strains. (b) Comparison of the fracture energy of PUU-$T_{0.6}D_{0.4}$-$I_{2.3}$ with other healable elastomers.[1-11]

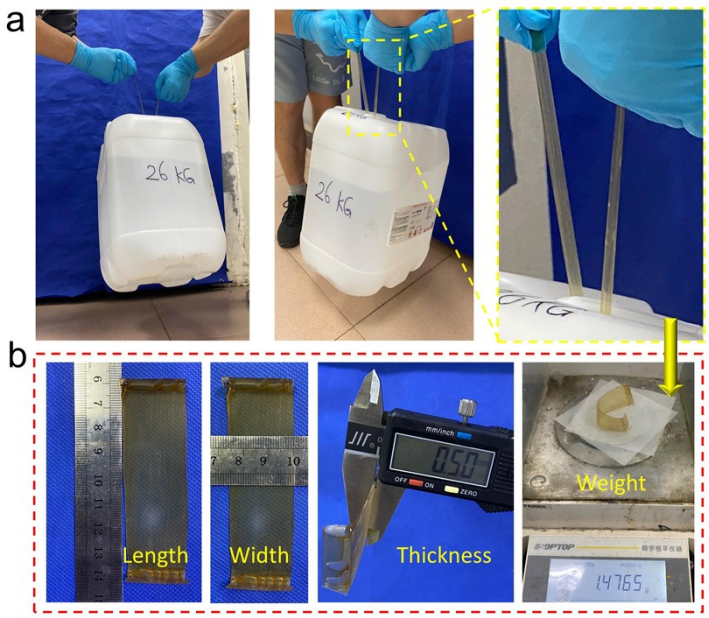

Figure S12 (a) Photographs showing that the PUU-$T_{0.6}D_{0.4}$-$I_{2.3}$ elastomer strip (1.5 g) can lift a weight of 26 kg. (b)Measure of length, width, thickness and weight of the PUU-$T_{0.6}D_{0.4}$-$I_{2.3}$ elastomer strip.

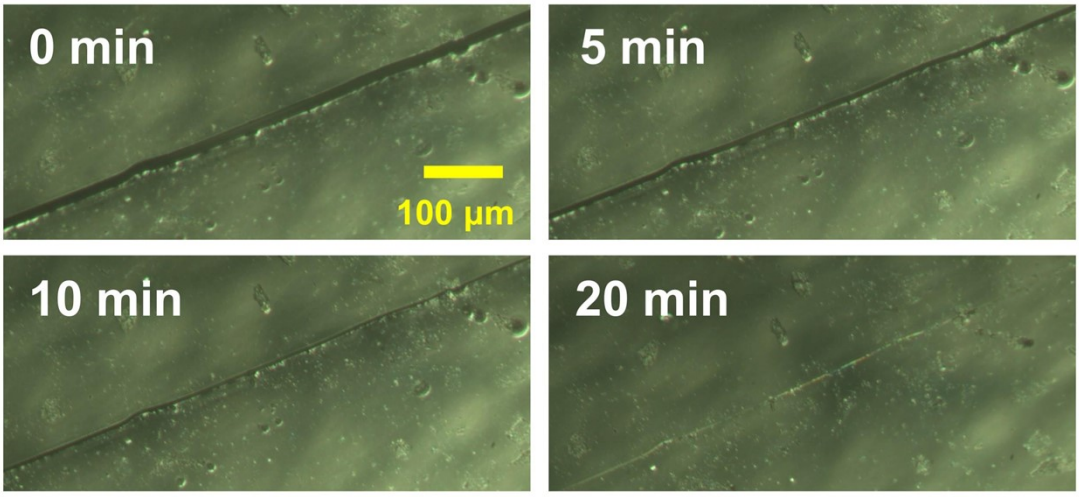

Figure S13 Optical microscopy images of the scratched PUU-$T_{0.6}D_{0.4}$-$I_{2.3}$ film in healing process at 80 ℃.

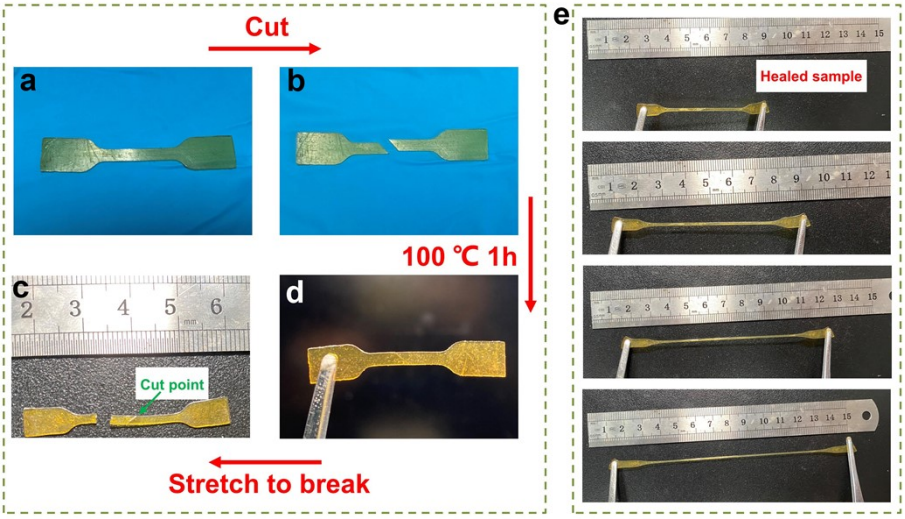

Figure S14 Photographs of (a) pristine sample, (b) cut sample, (c)healed sample after 1 h under 100 ℃, (d) broken sample after stretching and (e) process of stretching the healed sample.

Table S7 Healing efficiency of PUU-$T_{0.6}D_{0.4}$-$I_{2.3}$ under different healing conditions.

Healing condition	Tensile strength after healing (MPa)	Healing efficiency (%)	Strain-at-break after healing (%)	Healing efficiency (%)
60℃/12h	22.1 ± 2.6	29.4 ± 3.5	457.2 ± 25.4	64.3 ± 3.6
60℃/24h	34.8 ± 3.0	46.3 ± 4.0	505.5 ± 31.0	71.1 ± 4.4
85℃/2h	29.9 ± 5.2	39.8 ± 6.9	482.8 ± 25.9	67.9 ± 3.6
85℃/6h	41.2 ± 1.2	54.9 ± 1.6	637.4 ± 9.4	89.7 ± 1.3
85℃/12h	64.7 ± 4.6	86.1 ± 6.1	680.7± 31.8	95.7 ± 4.5
100℃/1h	53.7 ± 2.1	71.5 ± 2.8	689.5± 0.1	97.0 ± 0.0
100℃/2h	53.1 ± 3.1	70.6 ± 4.2	650.9 ± 19.9	91.5 ± 2.8

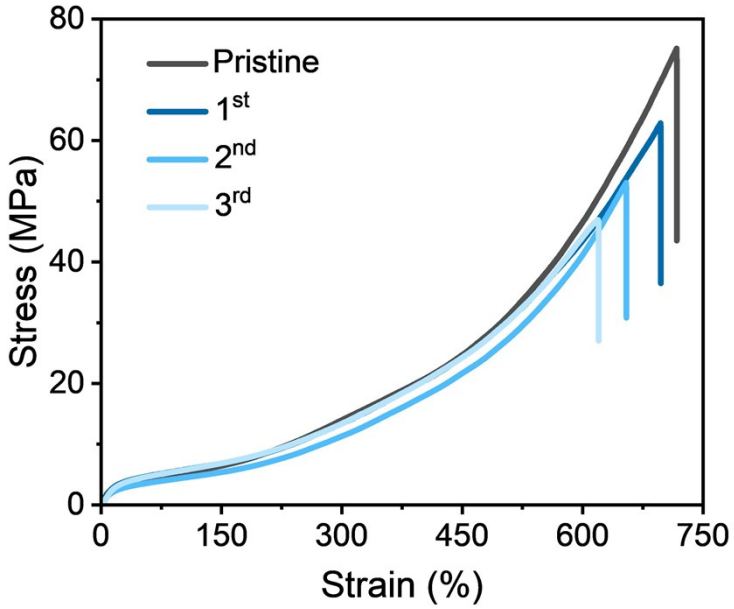

Figure S15 Stress-strain curves of PUU-$T_{0.6}D_{0.4}$-$I_{2.3}$ sample after cyclic cutting and healing.

Table S8 Summary of healing efficiency of tensile strength and strain at break of PUU-$T_{0.6}D_{0.4}$-$I_{2.3}$ sample after cyclic cutting and healing

	Healing efficiency (%)	
	Tensile strength	Strain at break
1st	83.6%	97.2%
2nd	80%	93.9%
3rd	84.5%	94.6%

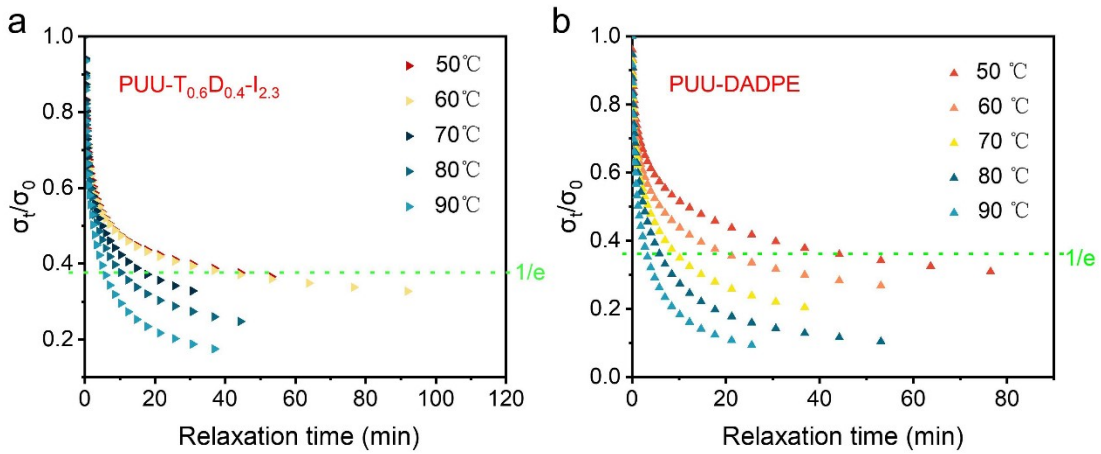

Figure S16 Normalized stress relaxation curves of (a) PUU-$T_{0.6}D_{0.4}$-$I_{2.3}$ and (b) PUU-DADPE samples subjected to a 10% strain under different temperatures.